

# A Reconfigurable All-Textile Wearable UWB Antenna

Antonio Di Natale and Emidio Di Giampaolo\*

**Abstract**—In this work a reconfigurable Ultra Wide Band (UWB) antenna for Wireless Body Area Network (WBAN) is presented. The antenna is completely composed of fabric materials and is able to switch its topology from a monopole-like structure (for on-body communications) to a microstrip-like structure (for off-body communications) maintaining UWB characteristic stable both on body and in free-space. This antenna presents good radiation properties in both configurations. In order to describe its time domain and frequency domain behavior, a System Fidelity Factor (SFF) analysis has been done for both topologies.

## 1. INTRODUCTION

All-textile Ultra Wide Band (UWB) antennas are becoming more and more attractive for on-body short range communication systems like wearable computing, sensor monitoring, health-care assistance, and in general for Wireless Body Area Network (WBAN) applications [1, 2]. Because of the easy integration in clothes, they permit to achieve comfortable wearability together with a robust assembly with the electronic circuitries for sensing, communications, wireless power transfer or energy harvesting [3, 4]. On the other hand, wearable antennas suffer from the coupling with the human body which may absorb a large part of the radiated electromagnetic field causing the mismatch of the antenna, reduction of efficiency, alteration of radiation pattern with respect to free space condition in addition to potential health risks in case of exposure for prolonged periods of time. For these reasons, planar shaped antennas are preferred because of the easy collocation on the human body while the use of a ground plane strongly reduces the absorption of energy in the body. Resorting to substrate integrated waveguide (SIW) technology the antennas shown in [3] and [5] achieve intrinsic shielding and stable characteristics in proximity of the human body even though the antennas are not UWB but narrow band or multiband.

The class of microstrip-like antennas instead [6–9], provided with full ground plane, allows low body-antenna interactions and is a good candidate for off-body communications in UWB-WBAN typical topology [1] thanks to its characteristics of directivity and good efficiency. The intrinsic drawback of this class of antennas is the narrow bandwidth based on resonance phenomena. Nevertheless, using suitable modifications and design shrewdness it is possible to extend the bandwidth to cover the entire FCC band. A first class of design methods consists in modifying the antenna geometry with a number of sub-structures having different resonant frequencies that partially overlap over the whole UWB. This is the case of [6] where folded parts and slots bring more resonances in the radiating patch while parasitic patches surrounding a shaped active one are used in [7], and a shaped multi-slot patch, instead, is proposed in [8]. Another design method concerns the use of a planar monopole combined with a reflector and a ground plane that permit to achieve unidirectional radiation pattern preserving the UWB bandwidth and shielding the human body [9].

The dipole-like family of wearable UWB antennas has the advantage of better yield in terms of time-domain performance [10] (e.g., the group delay and the so called System Fidelity Factor) with

---

*Received 12 March 2019, Accepted 5 May 2020, Scheduled 16 June 2020*

\* Corresponding author: Emidio Di Giampaolo (emidio.digiampaolo@univaq.it).

The authors are with the Department of Industrial and Information Engineering and Economics, University of L'Aquila, L'Aquila, Italy.

respect to multi-resonating antennas because a thick dipole (or monopole) is an intrinsic broadband antenna [11, 12]. Wide bandwidths, in fact, can be achieved with planar monopole antenna topology; therefore, it is frequently used in UWB communication systems. A recurrent design method is based on a flat monopole having various shapes fed by a microstrip line or a Coplanar Wave (CPW) line, e.g., circular disk [12], tapered triangular [13], and tapered slot [14]. An alternative design exploits the 3-D dimensions to develop compact broad band antennas like that based on a 3-D slot-loaded folded dipole shown in [15].

Despite the compact size typical of these antennas they have reasonable radiation performance and are frequently realized using rigid substrate, but better integration onto clothing has been obtained using flexible substrate [14, 16–19]. A limitation of flat monopole antennas is the alteration of the radiation diagram and impedance matching when they are worn, in particular for lying parallel to the surface of the body since in that collocation the antenna strongly feels the interaction of the electromagnetic field with the body.

On the other hand, it has been demonstrated in [20] that a proper choice of the radiation pattern and polarization of the transmitting and receiving antennas for the different body locations permits to optimize the WBAN system performance in terms of transmitted power and bit error rate. For on-body communications, it should be favourable to have the radiation pattern omnidirectional in the plane of the body while the polarization is vertical with respect to it. A monopole orthogonal to the body surface with a large ground plane is, evidently, a good candidate for this type of systems. In the case of off-body communications instead, unidirectional antennas are preferable because of the increased directivity while the use of a ground plane limits the losses in the body. Nevertheless, other interesting scenarios are possible.

In this work, we present an all-textile UWB wearable antenna for WBAN that allows to be reconfigured changing from a monopole-like shape to a microstrip-like shape. The change of configuration is simply obtained by raising and lowering a textile flap that contains the main radiating part of the antenna. It behaves like a monopole when being arranged orthogonally to the ground plane and like a microstrip patch when being placed parallel to the ground. In both configurations, the antenna preserves the UWB bandwidth while the radiation pattern changes according to the specific shape: omnidirectional and unidirectional in the cases of monopole and microstrip configurations, respectively.

The proposed antenna has been conceived to be used with a device that can switch between a tag mode and sensor mode. In tag mode, the flapping monopole acts as a UWB tag for localization and tracking of personnel, being omnidirectional. In sensor mode, the microstrip-like topology is a part of the air interface of wearable active and passive health sensors that exchange data with an interrogator, away from the body, under the user control.

Section 2 reports the structure of the antenna and the materials used for its realization. Section 3 shows the design method while Section 4 shows numerical results. In Section 5, measurement results of the antenna in free space and on-body conditions are reported. Finally, some conclusions are reported in Section 6.

## 2. ANTENNA STRUCTURE AND MATERIALS

The antenna is composed of four layers, a schema of the stratigraphy is shown in Fig. 1. From top to bottom, the first layer is made of conductive fabric, which consists of a CPW line that feeds a circular disk attached over a flapping layer. The flapping part can be rotated around a textile hinge orthogonal to the CPW line in order to accomplish both the monopole and microstrip topologies. A part of the ground plane is removed to house the flap when it lays down parallel to the ground in the microstrip topology.

The second layer is made of a textile fabric having thickness  $h_u$ , and this layer holds a reflector on the bottom side made of conductive fabric and connected to the ground of the CPW line. The reflector has the main function of matching the antenna's impedance in the microstrip topology; nevertheless, it also affects the radiation pattern as will be shown later. The third layer is made of textile fabric with thickness  $h_d$  while the last layer is a reflecting ground made of conductive fabric.

The drawing of the antenna functioning as a monopole is shown in Fig. 2(a), while the microstrip-like configuration is shown in Fig. 2(b). Table 1 reports the corresponding dimensions in millimeters.

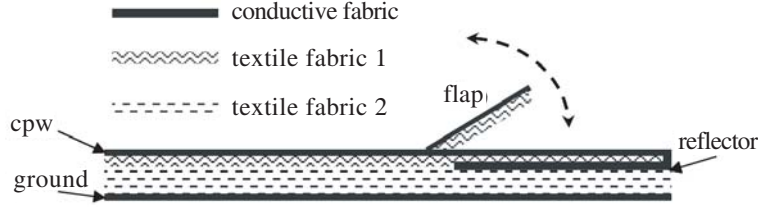


Figure 1. Schema of the side view of the antenna.

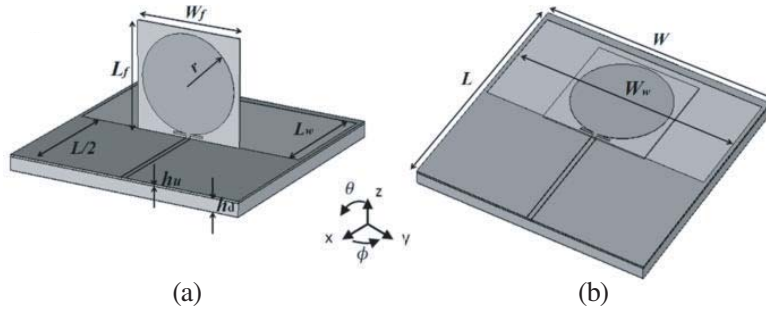


Figure 2. Antenna's drawings: (a) monopole configuration; (b) microstrip-like configuration.

Table 1. Optimized geometrical values of antenna parts.

$W$	$L$	$W_w$	$L_w$	$W_f$	$L_f$	$r$	$h_u$	$h_d$
90	90	87	42	40	40	18.3	0.6	4.8

The used conductive textile material is the ShieldIt Super which has surface resistivity less than 0.07 Ohm/sq and is 0.17mm thick [21]. Different textile fabrics can be used for the two dielectric layers, and we have designed and experimented two different setups: the first uses denim for the first layer and felt for the second one; the other setup, instead, uses denim for both layers. Simulation and experimental measurements have shown similar results in terms of bandwidth and radiation patterns once the thickness and antenna's dimensions have been optimized. Nevertheless, the use of felt makes the antenna more prone to deformations and mechanical instability (e.g., disjunction of connector) because the felt is softer than denim so that we prefer to use the second setup, and we refer to it from now on. The dielectric properties of the used denim are extrapolated using the ring resonator technique [22]: its dielectric constant and loss tangent values are, respectively, 1.43 and 0.036, measured at 5 GHz. For the first layer, we use a denim fabric having thickness 0.6 mm, and the thickness of the fourth layer ( $h_d$ ), instead, is a parameter to be optimized since it affects the behavior of the antenna, in particular the gain.

To realize the optimized thickness, more fabrics have been sewn on top of each other. The flapping part that allows the change from one topology to the other has been made with denim fabric 0.6 mm thick and with a small prism of very light foam. The prism of foam has dielectric constant very close to one and serves to support the flap in the upright position. It acts, in fact, as a spring that is compressed with thin thickness in the case of microstrip-like configuration instead, and it splays and supports, in an almost orthogonal position, the flap in the case of monopole configuration.

### 3. ANTENNA DESIGN

The design of the antenna has been performed subdividing the task into two almost independent parts: one for monopole topology and one for microstrip topology. In fact, the design of microstrip topology is subsequent to that of the monopole that remains invariant apart from the lying. The electromagnetic

analysis has been performed with Ansys HFSS [23] while the optimization of the design of the structures of the antenna has been performed with a genetic algorithm.

### 3.1. Monopole Topology

A circular disk orthogonal to a ground plane is an intrinsic broadband radiating structure. When it is CPW-fed the main parameters to optimize the bandwidth are the radius  $r$  of the disk that limits the lower frequency of the band, the gap  $g$  from the ground plane that has most effects at higher frequencies, and the width of the ground plane  $W$ . Since the increase of the size of ground plane gives negligible effects on the monopole behavior after a certain size while it is an important design parameter for the microstrip topology, we do not consider it as a design parameter of the monopole and assume that it is large enough to not affect the monopole behaviour. The dimension  $W$  is determined in the design phase of the microstrip topology making a check of the behavior of the monopole a-posteriori.

Since the fabric in the nearness of the hinge of the flap is subjected to bulge when the flap commutates between monopole and microstrip configurations, the gap  $g$  might be slightly variable. As a consequence, the bandwidth may become unstable changing every time the flap moves. To avoid that drawback, we introduce, in the design of the monopole, a couple of thin strips connected orthogonally to the feed line and placed at the intersection point between the disk and the coplanar line. That structure makes the impedance matching of the monopole insensitive to possible variations of the gap but introduces an upper limit to the bandwidth. The length  $L_s$  of the strips is the main design parameter that determines the upper frequency, and Fig. 3 shows the details of the structure.

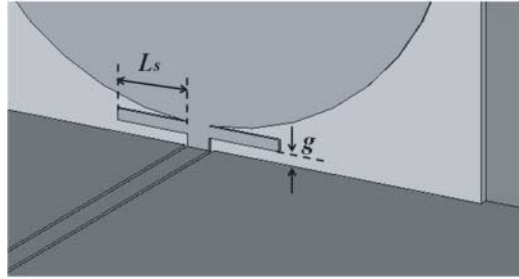


**Figure 3.** Geometric details of monopole disk.

The impedance matching of the monopole is independent from the shape and extension of the ground plane opposite to the driven line, i.e., the part of ground plane without the CPW line in Fig. 2(a). For that reason, the part of the ground plane behind the monopole is free to be modified and can host the microstrip part of the antenna. Nevertheless, the radiating characteristics feel the absence of that part of ground plane mainly at lower frequencies, so a floating ground plane is introduced at the bottom side of fourth layer in order to compensate the lack of that part of CPW ground and to improve the shielding of the body from the electromagnetic field.

Table 1 shows the optimized values (mm) of the main design parameters in order to achieve the UWB bandwidth.

### 3.2. Microstrip Topology

When the denim flap, which contains the radiator disk, is put parallel to the substrate over the CPW ground plane, the input impedance mismatches at some frequency sub-bands. To obtain the UWB bandwidth without changing the geometry of the monopole, the coplanar ground plane has been narrowed along the sides of the substrate in the part opposite to the driven line (Fig. 2(b)), extended to the back of the top substrate and connected to a shaped reflector that behaves like a broad band matching structure (Fig. 1.) The reflecting structure is placed at the interface between two textile substrates that have suitable thickness. The thickness ( $h_u$ ) of the first substrate is kept constant while

the thickness of the second substrate ( $h_d$ ) has been optimized in order to increase the gain of the antenna in that topology.

The geometry of reflector is shown in Fig. 4, and it consists of a main part having the shape of two opposite triangles (like a bowtie) which are connected together by means of a broad line. The line has two large strips orthogonal to its axis and is connected to the coplanar ground plane. The main design parameters that permit the UWB impedance matching are the lengths of the height  $h$  and base  $b$  of the triangles, the width  $w_s$  and length  $l_s$  of the strips, the position  $d_p$  of the strips, and the length  $l_p$  of the line. The dimensions of these parameters (mm, Table 2) have been obtained by means of an optimization having the objective to enlarge the bandwidth as much as possible. That shaping of the reflector permits to achieve a UWB bandwidth apart from some frequencies where the reflection coefficient exceeds the  $-10$  dB threshold. To flat the exceeding parts, we punch each triangle with four scaled triangular slots that form a Sierpinsky-like structure. The dimensions of the slots have been obtained after an optimization aimed to flat the reflection coefficient.

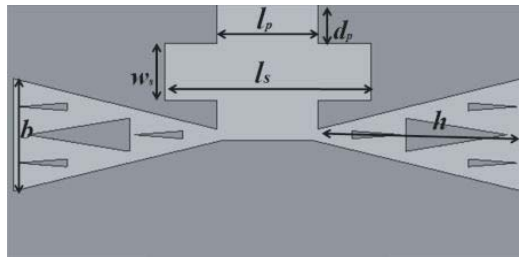


Figure 4. Geometric details of shaped reflector.

Table 2. Optimized geometrical dimensions of the reflector parts.

$g$	$L_s$	$h$	$b$	$w_s$	$l_s$	$d_p$	$l_p$
0.9	5	34	18.6	9.5	34.3	6.4	16.8

#### 4. NUMERICAL RESULTS

The optimization of the antenna model and the analysis of its behavior in each topology have been performed in free-space, while an a-posteriori check has been performed to test the antenna on body. For on-body simulations, we use an equivalent homogeneous body model [26, 27] having volume  $130 \times 120 \times 44 \text{ mm}^3$  and simulating a muscle tissue with relative dielectric constant 50 and conductivity 3 S/m. For both topologies, the antenna is centered above the tissue model at a distance of 10 mm that approximates the presence of clothes on the body. Because of the ground plane, simulation results show that the antenna is insensitive to the body so that the behaviors in terms of reflection coefficient and radiation pattern do not change significantly with or without the body.

Since the design of the monopole topology does not require particular efforts, we report the obtained results in terms of reflection coefficient and radiation pattern without the description of the evolution of the design. The microstrip-like topology instead requires more design steps and electromagnetic shrewdness; therefore, we report intermediate results in order to give an in-depth description of the evolution of the design.

##### 4.1. Reflection Coefficient

The reflection coefficient of the monopole antenna is shown in Fig. 5. Practically, it is insensitive to the floating ground plane. Fig. 6 shows the reflection coefficient for different lengths ( $L_s$ ) of the strips placed near the radiating disk. The upper limit of the frequency band is sensitive to the length of the strips, and in particular the upper limit decreases if the length of the strip is increased. For the selected

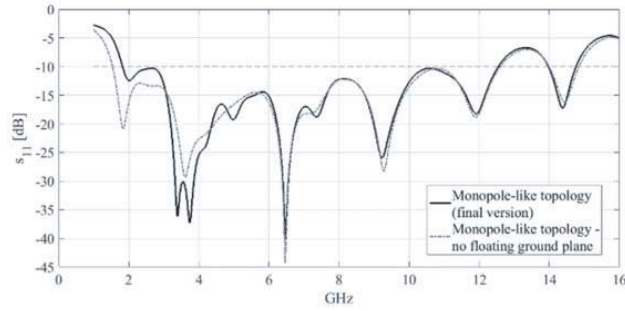


**Figure 5.** Reflection coefficient of the monopole-like antenna: comparison between the final version of the antenna and the final version of the antenna without floating ground plane.

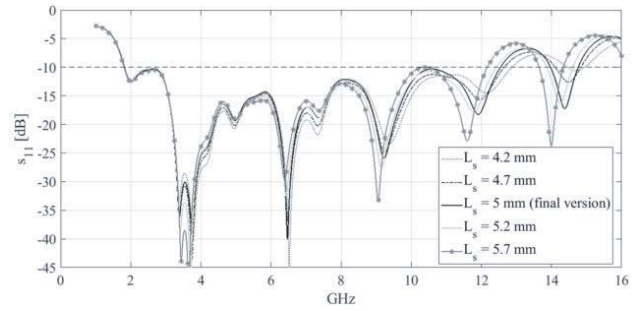


**Figure 6.** Reflection coefficient of the monopole topology for different lengths of the strips.

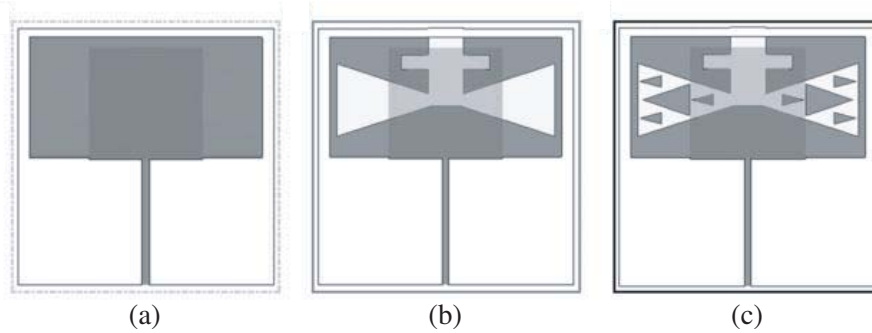


**Figure 7.** Design steps of the microstrip-like antenna (radiating disk hidden): (a) the radiating disk lies over a rectangular aperture of the CPW ground; (b) shaped reflector connected to ground; (c) final structure with punched reflector.

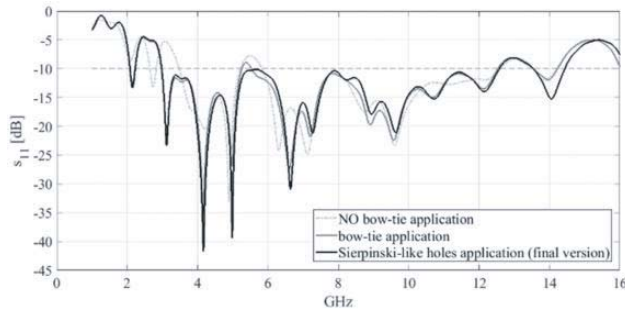


**Figure 8.** Evolution of the reflection coefficient of the microstrip-like antenna for the design steps shown in Fig. 7.

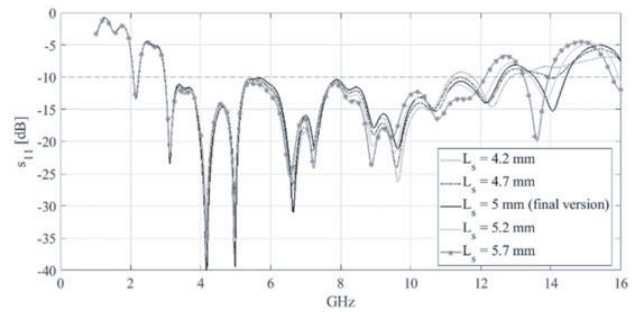


**Figure 9.** Reflection coefficient of the microstrip-like antenna for different lengths of the strips near the radiating disk.

length, we obtain a UWB impedance matching larger than the FCC regulations: from 1.82 GHz to 12.55 GHz.

The steps of the design procedure of the microstrip-like antenna are shown in Fig. 7. The first step (Fig. 7(a)) considers the radiating disk, designed for the monopole topology, which is lying over the denim substrate inside a rectangular aperture of the coplanar ground that forms a frame along the sides of the substrate. The corresponding reflection coefficient shown in Fig. 8 (dotted line) shows two useful bands: one around 4 GHz and the other from about 6 to 10 GHz. The second step introduces, inside the aperture and in the bottom side of the substrate, a reflector having the shape of a bowtie (Fig. 7(b)).

Several alternative shapes have been simulated obtaining a reflection coefficient worse than the case without the reflector (first step). Instead, the bowtie-shaped reflector permits to improve the matching even though the reflection coefficient is larger than the threshold  $-10$  dB over some narrow sub-bands (dashed dotted line in Fig. 8). The third step introduces a set of slots punched on the reflector, and the effect of the slots permits to match the antenna over the full band from 2.98 GHz to 12.57 GHz. Finally, the variation of the reflection coefficient because of the change of the length of the strips ( $L_s$ ) on the radiating disk is shown in Fig. 9. Similar to the monopole topology, the increase of the length of the strips makes the upper frequency of the band smaller.

### 4.2. Radiation Pattern

The 3-D gain patterns of the optimized monopole and microstrip-like topologies together with the corresponding current density over the main radiator are shown in Fig. 10 and Fig. 11, respectively. The gain patterns on ( $z-x$ ) plane (i.e.,  $\phi = 0^\circ$ ) of the optimized antennas are shown in Fig. 12 for (a) monopole (b) microstrip topologies, at three different frequencies (4.2 GHz, 6.6 GHz, 9.6 GHz). The monopole patterns are almost omnidirectional at lower frequencies while the microstrip-like patterns show higher gain values at slant directions. Figs. 13(a) and (b) show the gain patterns on a plane parallel to ( $z-y$ ) (i.e.,  $\phi = 130^\circ$ ) for (a) monopole and (b) microstrip-like topologies, respectively. Fig. 14 shows the variation of the maximum gain vs. frequency, and it oscillates between 2 dB and 6 dB in the case of (a) monopole, and between 2 dB and 8 dB for (b) microstrip topologies.

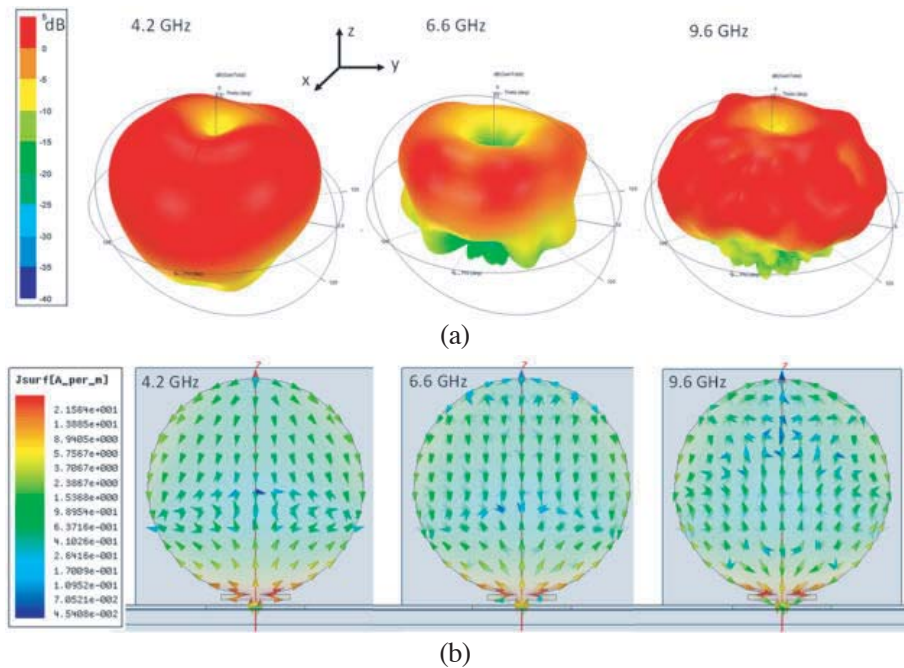


**Figure 10.** (a) 3-D gain patterns and (b) corresponding current distribution for monopole topology at three different frequencies.

For microstrip-like topology, the main component contributing to the total gain is the  $\theta$  component apart from three narrow sub-bands near 4 GHz, 6.3 GHz, and 7.8 GHz. This means that single polarization across the most part of UWB is obtained. In monopole-like topology, instead, both  $\theta$  and  $\phi$  components of the gain contribute to the total gain apart from four narrow sub-bands where the  $\theta$  component is dominant.

The effect of the thickness of the substrates has been analysed and shown in Fig. 15–Fig. 17. It is possible to observe that only the thickness of the second substrate has an important effect on the gain of microstrip topology especially at lower frequencies (Fig. 17). The thickness of  $h_d = 4.8$  mm has been chosen because it gives a good trade-off between low and high frequencies.

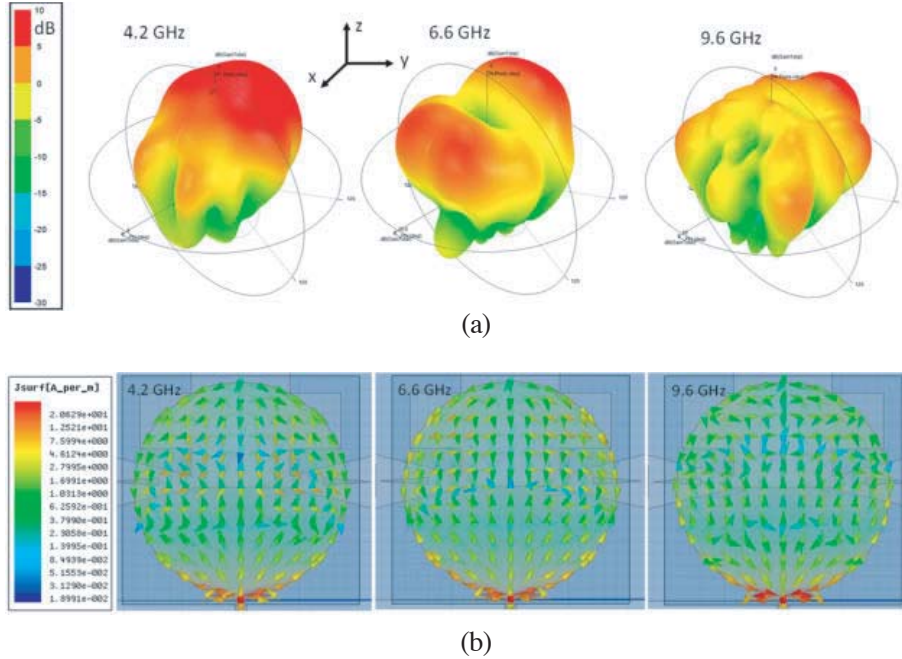


**Figure 11.** (a) 3-D gain patterns and (b) corresponding current distribution for microstrip-like topology at three different frequencies.

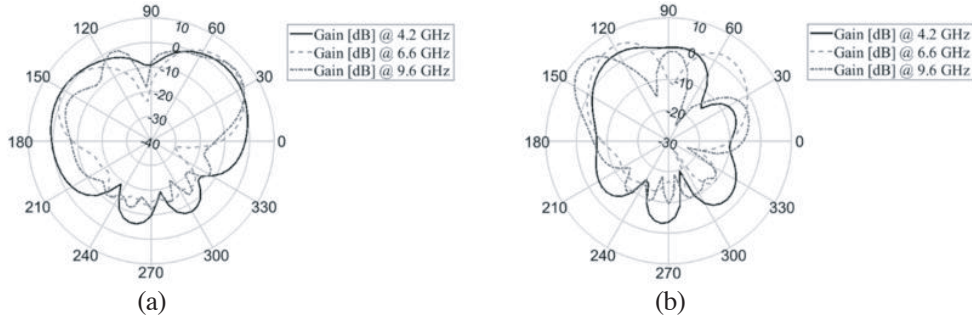


**Figure 12.** Gain patterns for (a) monopole and (b) microstrip-like topologies at three different frequencies (continuous line @ 4.2 GHz, dashed line @ 6.6 GHz and dotted line @ 9.6 GHz). Cutting plane ( $z$ - $x$ ).

### 4.3. System Fidelity Factor Analysis

In order to estimate the goodness of the designed antennas, we simulate the System Fidelity Factor (SFF) in agreement with the procedure [10] that defines the normalized cross-correlation between a transmitted UWB pulse  $\hat{T}_S(t)$  and its received version  $\hat{R}_S(t + \tau)$ :

$$0 \leq SFF = \max \int_{-\infty}^{+\infty} \hat{T}_S(t) \hat{R}_S(t + \tau) dt \leq 1 \quad (1)$$

The SFF value strongly depends on the system transfer function  $H(\omega)$ , defined as:

$$H(\omega) = H_{Tx} H_{CH} H_{Rx} \quad (2)$$

where  $H_{Tx}$ ,  $H_{CH}$ , and  $H_{Rx}$  are respectively the transmitting antenna transfer function, channel transfer function, and receiving antenna transfer function. The used SFF scenario consists of two equal antennas (i.e., same topology) placed at a distance of 0.5 m, and one is stationary while the other is rotating

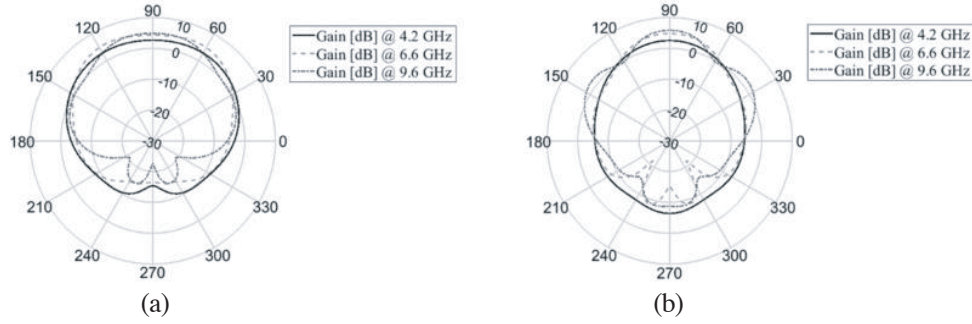


**Figure 13.** Gain patterns for (a) monopole and (b) microstrip-like topologies at three different frequencies (continuous line @ 4.2 GHz, dashed line @ 6.6 GHz and dotted line @ 9.6 GHz). Cutting plane parallel to  $(z-y)$ .

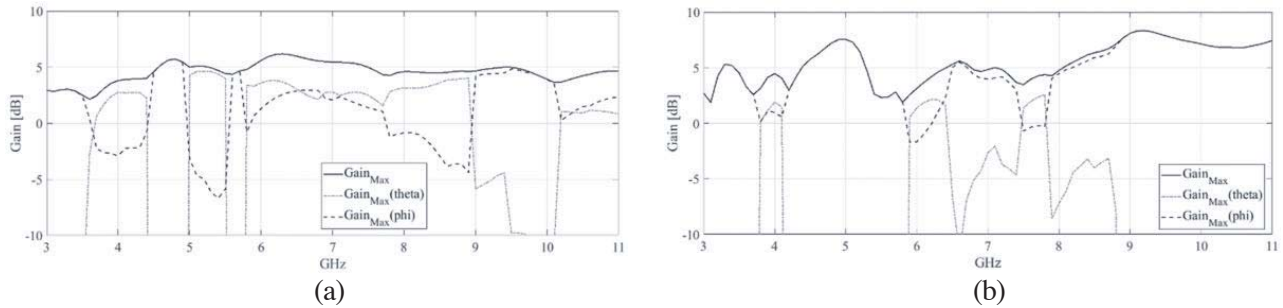


**Figure 14.** Maximum gain vs. frequency for (a) monopole and (b) microstrip topologies. Continuous line total gain; dash-dotted and dashed lines  $\phi$  and  $\theta$  components, respectively.

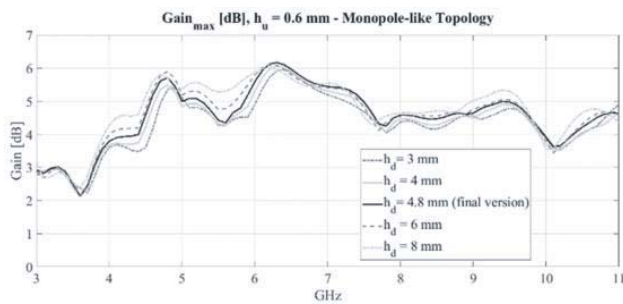


**Figure 15.** Maximum gain vs. frequency in case of monopole topology for different thickness of second substrate.

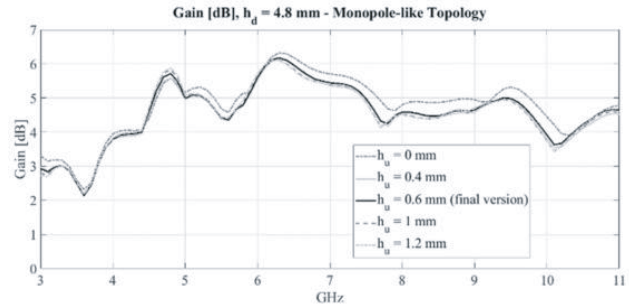


**Figure 16.** Maximum gain vs. frequency in case of monopole topology for different thickness of first substrate.

around the axis orthogonal to the direction of maximum radiation. A sine-modulated Gaussian pulse is transmitted from the stationary antenna

$$T_s(t) = e^{-((t-a\cdot\tau)/\tau)^2} \cdot \sin(2\pi f_r \cdot (t - a \cdot \tau)) \tag{3}$$

with  $\tau = 210$  ns,  $a = 3$ ,  $f_r = 4.5$  GHz.

The results of this analysis give the SFF for different angles of rotation, and it is shown in Fig. 19 for both topologies. For the microstrip-like topology, the SFF value is between 0.39 (at  $\pm 145^\circ$  rotation angle) and 0.77 (at  $\pm 35^\circ$  rotation angle), while for the monopole topology, the SFF value is between 0.52 (at  $0^\circ$  rotation angle) and 0.9 (at  $\pm 65^\circ$  rotation angle).

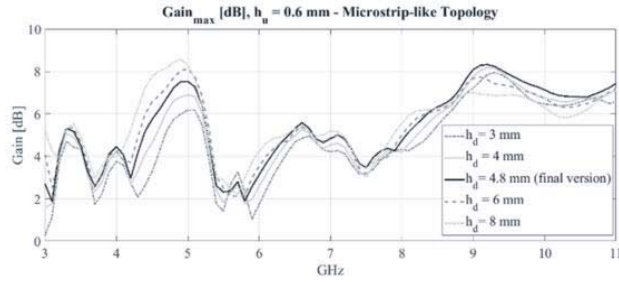


**Figure 17.** Maximum gain vs. frequency in case of microstrip-like topology for different thickness of second substrate.

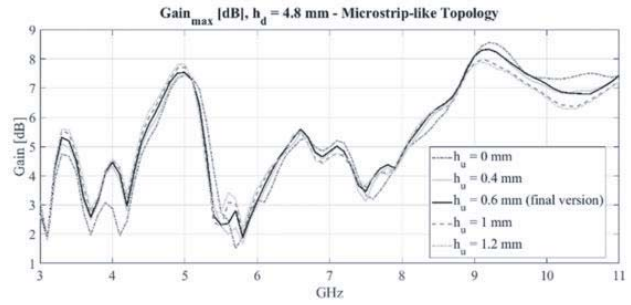


**Figure 18.** Maximum gain vs. frequency in case of microstrip-like topology for different thickness of the first substrate.

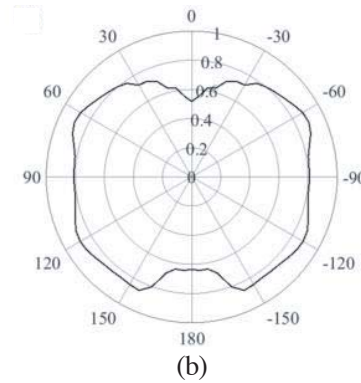
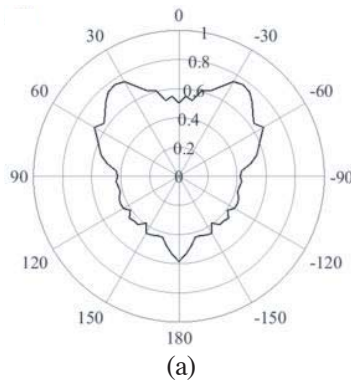


**Figure 19.** Simulated system fidelity factor results: (a) microstrip-like topology; (b) monopole topology.

## 5. MEASUREMENT RESULTS

The realized prototype antenna is hand-made, and all conductive parts are fixed to the fabric substrates by ironing, while the SMA connector is soldered. A picture of the realized antenna is shown in Fig. 20. The measurements of the reflection coefficient have been performed with Anritsu MS46122B vector network analyzer.

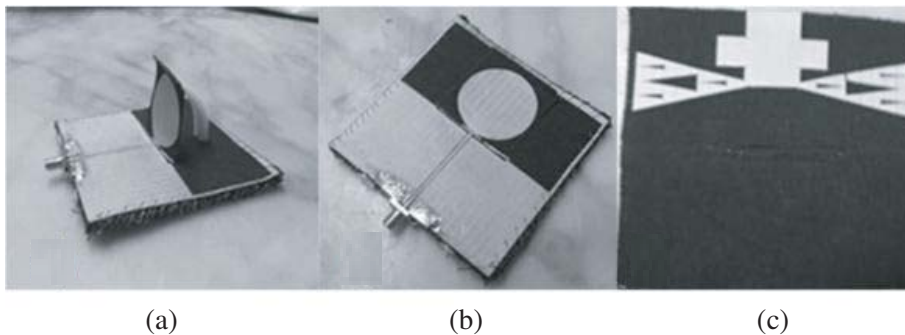


**Figure 20.** Realized prototype antenna: (a) monopole configuration; (b) microstrip configuration; (c) underlying shaped reflector.

### 5.1. Reflection Coefficient

Reflection coefficient measurements have been performed in a laboratory environment with the antenna placed over a hollow cardboard box and, for on-body measurement, over a phantom, far from scattering objects. The phantom has been realized with a very thin plastic box filled with a solution of distilled water and 0.9% sodium chloride. Additional measurements with the antenna placed on an arm and on the chest of a volunteer have been performed.

The reflection coefficient of the antenna alone and on phantom together with the corresponding simulated result is shown in Fig. 21 for monopole topology and Fig. 22 for microstrip topology.

The measured reflection coefficient of monopole configuration has a  $-10$  dB bandwidth from 2.62 GHz to 10.1 GHz apart from a slight impedance mismatching near 3 GHz where it is  $-9$  dB for a sub-band of about 30 MHz. The measured bandwidth for microstrip-like topology spans from 2.73 GHz to 10.1 GHz with a slight mismatch for sub-band of about 35 MHz near 5 GHz. For both configurations, negligible differences are visible between the alone and on-body measurements. In comparison with simulated results, the measured bandwidths have the upper limit about 1.5 GHz lower than the simulated one. That difference is mainly dependent on the manufacturing inaccuracy of the hand-made prototype: since the reduction of the bandwidth is at higher frequency and has the same value for both configurations, it depends on a part of the antenna common to both configurations. After some checks, we have found that it depends on the quality of the soldering of the connector that has main effects at higher frequencies. The behavior of the monopole configuration does not change for slant positions of the flapping part (i.e., the monopole is not exactly orthogonal to the ground plane). Furthermore, the whole behavior of the antenna does not change for moderate bending of its structure.

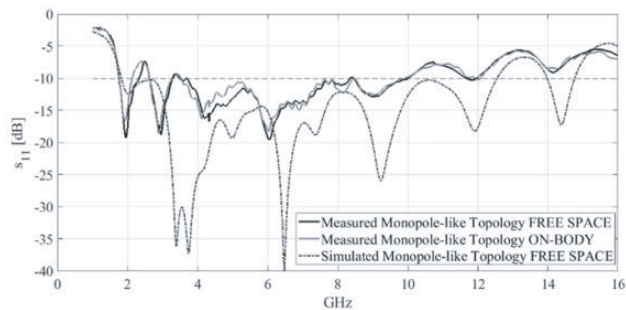


**Figure 21.** Measured reflection coefficient of monopole topology for the antenna alone (continuous line), on phantom (dashed) and simulated (dash-dotted).

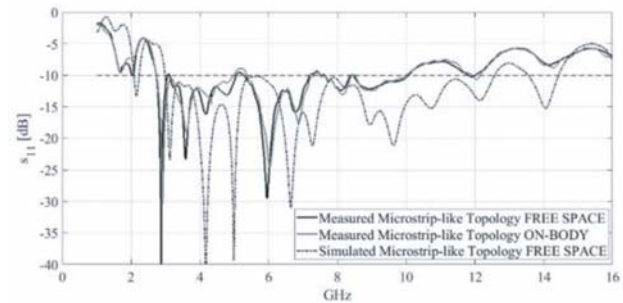


**Figure 22.** Measured reflection coefficient of microstrip topology for the antenna alone (continuous line), on phantom (dashed) and simulated (dash-dotted).

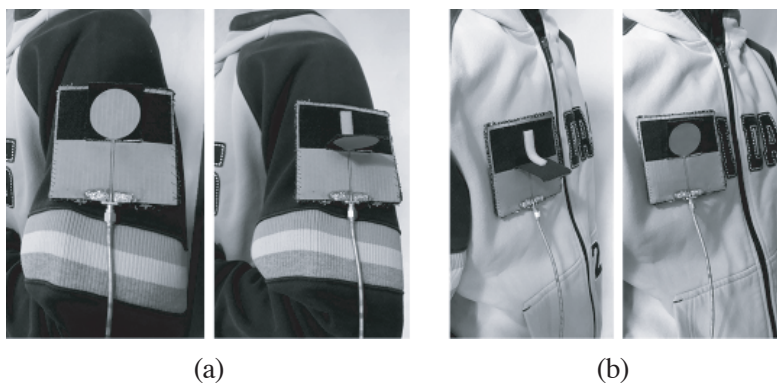


**Figure 23.** On-body measurement set-up for both antenna topologies: (a) antenna on an arm; (b) antenna on the chest.

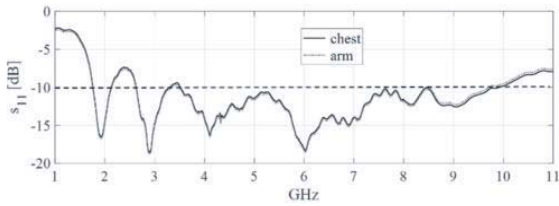


**Figure 24.** On-body measured reflection coefficient for monopole topology.

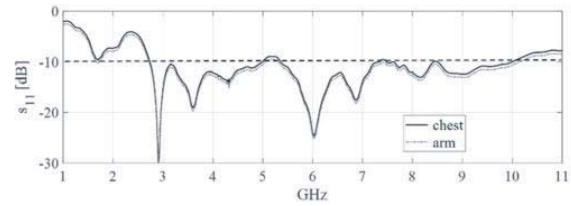


**Figure 25.** On-body measured reflection coefficient for microstrip-like topology.

Fig. 23 shows the antenna worn on the chest and on an arm where it is moderately bent, and the corresponding reflection coefficients for the two antenna configurations do not change significantly as shown in Fig. 24 and Fig. 25.

## 6. CONCLUSIONS

A UWB wearable all-textile antenna able to be reconfigured between a monopole and a microstrip-like antenna has been proposed and discussed. It is based on a circular radiating disk that works as a monopole when being placed orthogonally to a ground plane and as a microstrip patch when it is lying parallel to a modified ground plane. Numerical analysis shows that both topologies have satisfactory UWB characteristic with bandwidth compliant with FCC regulation and a fair system fidelity factor that allows the antenna as an air interface for wearable sensors and short range communication devices.

## REFERENCES

1. Yan, S., P. J. Soh, and G. A. E. Vandenbosch, "Wearable ultrawideband technology — A review of ultrawideband antennas, propagation channels, and applications in wireless body area networks," *IEEE Access*, Vol. 6, 42177–42185, Jul. 2018.
2. Ghosh, D. and P. K. Sahu, "UWB in healthcare," *International Conference on Electromagnetics in Advanced Applications (ICEAA)*, 679–682, Cairns, QLD, 2016.
3. Lemey, S., F. Declercq, and H. Rogier, "Dual-band substrate integrated waveguide textile antenna with integrated solar harvester," *IEEE Antennas Wirel. Propag. Lett.*, Vol. 13, 269–272, 2014.
4. Dierck, A., H. Rogier, and F. Declercq, "A wearable active antenna for global positioning system and satellite phone," *IEEE Trans. Antennas Propag.*, Vol. 61, No. 2, 532–538, Feb. 2013.
5. Moro, R., S. Agneessens, H. Rogier, and M. Bozzi, "Wearable textile antenna in substrate integrated waveguide technology," *IET Electron. Lett.*, Vol. 48, No. 16, 985–987, Aug. 2012.
6. Kang, C.-H., S.-J. Wu, and J.-H. Tarng, "A novel folded UWB antenna for wireless body area network," *IEEE Trans. Antennas Propag.*, Vol. 60, No. 2, 1139–1142, Feb. 2012.
7. Samal, P. B., P. J. Soh, and G. A. E. Vandenbosch, "A systematic design procedure for microstrip-based unidirectional UWB antennas," *Progress In Electromagnetics Research*, Vol. 143, 105–130, 2013.
8. Samal, P. B., P. J. Soh, and Z. Zakaria, "Compact and wearable microstrip-based textile antenna with full ground plane designed for WBAN-UWB 802.15.6 application," *European Conference on Antennas and Propagation (EuCAP)*, 2019.
9. Poffelie, L. A. Y., P. J. Soh, S. Yan, and G. A. E. Vandenbosch, "A high fidelity all-textile UWB antenna with low back radiation for off-body WBAN applications," *IEEE Trans. Antennas Propag.*, Vol. 64, No. 2, 757–760, Feb. 2016.
10. Quintero, G., J.-F. Zürcher, and A. K. Skrivervik, "System fidelity factor: A new method for comparing UWB antennas," *IEEE Trans. Antennas Propag.*, Vol. 59, No. 7, 2502–2512, Jul. 2011.

11. Dumoulin, A., M. John, M. J. Ammann, and P. McEvoy, "Optimized monopole and dipole antennas for UWB asset tag location systems," *IEEE Trans. Antennas Propag.*, Vol. 60, No. 6, 2896–2904, Jun. 2012.
12. Liang, J., L. Guo, C. C. Chiau, X. Chen, and C. G. Parini, "Study of CPW-fed circular disc monopole antenna for ultra wideband applications," *IEE Proceedings — Microwaves, Antennas and Propagation*, Vol. 152, No. 6, 520–526, Dec. 9, 2005.
13. Verbiest, J. R. and G. A. E. Vandenbosch, "A novel small-size printed tapered monopole antenna for UWB WBAN," *IEEE Antennas Wirel. Propag. Lett.*, Vol. 5, No. 1, 377–379, Dec. 2006.
14. Ur-Rehman, M., Q. H. Abbasi, M. Akram, and C. Parini, "Design of band-notched ultra wideband antenna for indoor and wearable wireless communications," *IET Microw., Antennas Propag.*, Vol. 9, No. 3, 243–251, 2015.
15. Mobashsher, A. T. and A. M. Abbosh, "Compact 3-D slot-loaded folded dipole antenna with unidirectional radiation and low impulse distortion for head imaging applications," *IEEE Trans. Antennas Propag.*, Vol. 64, No. 7, 3245–3250, Jul. 2016.
16. Sun, Y., S. W. Cheung, and T. I. Yuk, "Design of a textile ultra-wideband antenna with stable performance for body-centric wireless communications," *IET Microw., Antennas Propag.*, Vol. 8, No. 15, 1363–1375, 2014.
17. Klemm, M., I. Z. Kovcs, G. F. Pedersen, and G. Troster, "Novel small-size directional antenna for UWB WBAN/WPAN applications," *IEEE Trans. Antennas Propag.*, Vol. 53, No. 12, 3884–3896, Dec. 2005.
18. Balarami Reddy, B. N., P. Sandeep Kumar, T. Rama Rao, N. Tiwari, and M. Balachary, "Design and analysis of wideband monopole antennas for flexible/wearable wireless device applications," *Progress In Electromagnetics Research M*, Vol. 62, 167–174, 2017.
19. Osman, M. A. R., M. K. A. Rahim, N. A. Samsuri, H. A. M. Salim, and M. F. Ali, "Embroidered fully textile wearable antenna for medical monitoring applications," *Progress In Electromagnetics Research*, Vol. 117, 321–337, 2011.
20. See, T. S. P., T. M. Chiam, M. C. K. Ho, and M. R. Yuce, "Experimental study on the dependence of antenna type and polarization on the link reliability in on-body UWB systems," *IEEE Trans. Antennas Propag.*, Vol. 60, No. 11, 5373–5380, Nov. 2012.
21. [https://www.lessemf.com/shieldit\\_super.pdf](https://www.lessemf.com/shieldit_super.pdf).
22. Heinola, J.-M. and K. Tolsa, "Dielectric characterization of printed wiring board materials using ring resonator techniques: A comparison of calculation models," *IEEE Transactions on Dielectrics and Electrical Insulation*, Vol. 13, No. 4, 717–726, Aug. 2006.
23. [ansys.com/Products/Electronics/ANSYS-HFSS](https://www.ansys.com/Products/Electronics/ANSYS-HFSS).
24. Chahat, N., M. Zhadobov, R. Sauleau, and K. Ito, "A compact UWB antenna for on-body applications," *IEEE Trans. Antennas Propag.*, Vol. 59, No. 4, 1123–1131, Apr. 2011.
25. Elaziz, N. M. A., A. J. Alzubaidi, and M. A. Hassan, "Performance of the 6th derivative gaussian UWB pulse shape in IEEE802.15.3a multipath fading channel," *IOSR Journal of Engineering*, Vol. 04, No. 12, 1–12, ISSN (e): 2250-3021, ISSN (p): 2278-8719, Dec. 2014.
26. Alighanbari, A. and C. D. Sarris, "Parallel time-domain full-wave analysis and system-level modeling of ultrawideband indoor communication system," *IEEE Trans. Antennas Propag.*, Vol. 57, No. 1, 231–240, Jan. 2009.
27. Klemm, M. and G. Troester, "Textile UWB antennas for wireless body area networks," *IEEE Trans. Antennas Propag.*, Vol. 54, No. 11, 3192–3197, Nov. 2006.